Journal of Solid State Chemistry 182 (2009) 1265–1272

Contents lists available at ScienceDirect

Journal of Solid State Chemistry

journal homepage: www.elsevier.com/locate/jssc

Single-crystalline α-Fe_2O_3 with hierarchical structures: Controllable synthesis, formation mechanism and photocatalytic properties

Jianmin Gu, Siheng Li, Enbo Wang *, Qiuyu Li, Guoying Sun, Rui Xu, Hong Zhang

Key Laboratory of Polyoxometalate Science of Ministry of Education, Department of Chemistry, Northeast Normal University, Changchun, Jilin 130024, People's Republic of China

ARTICLE INFO

Article history:
Received 21 November 2008
Received in revised form
16 January 2009
Accepted 26 January 2009
Available online 12 February 2009

Keywords:
Hematite
Hierarchical structures
Photocatalytic properties

ABSTRACT

A dual iron precursors system in a hydrothermal process was developed for controllable fabrication of α-Fe_2O_3 hierarchical structures with different morphologies. Micro-pines, snowflakes and bundles were successfully synthesized simply by tuning the total concentration of the two iron precursors $K_4[Fe(CN)_6]$ and $K_3[Fe(CN)_6]$ and their molar ratio. The obtained α-Fe_2O_3 hierarchical structures were characterized using field-emission scanning electron microscopy, transmission electron microscopy, X-ray powder diffraction, X-ray photoelectron spectroscopy and energy-dispersive X-ray analysis. The effect of experimental conditions on the morphologies of the α-Fe_2O_3 crystals was systematically investigated. A possible formation mechanism of different α-Fe_2O_3 hierarchical structures was proposed. Good photocatalytic properties were observed for all the hierarchical structures.

1. Introduction

Nanomaterials with a hierarchical structure have attracted intensive research attention. Their complicated structures are usually concomitant with diverse characteristics, thus having various applications. With the high surface area specific for nanomaterials [1], these hierarchical structures often grow into micrometer-scaled materials, bearing the mechanical robustness desired in various fields. Recently, nanomaterials with various hierarchical morphologies [2–7] have been synthesized and successfully used in catalysis and environmental improvement, and as sensors in biological systems. Template methods [8], thermal evaporation [9], electrochemical deposition [10], chemical vapor deposition [11] and hydrothermal synthesis [12] are the common methods to prepare this kind of materials. Among these methods, hydrothermal process bears the advantage that it can initiate the nucleation in the growth of micro- and nano-crystals, and promote the formation of crystalline products to completion under non-equilibrium conditions [13]. This method has been widely used in preparing various hierarchical structures [14].

Hematite (α-Fe_2O_3) is the most stable iron oxide with n-type semiconducting properties (band gap $E_g = 2.1$ eV) at ambient conditions [15]. Its potential applications have been explored in fields including photocatalysis [16], gas sensors [17], lithium ion battery [18] and magnetic materials production [19]. α-Fe_2O_3 nano-crystals with various morphologies such as urchinlike [20], quasicubic [21], belts [22], tubes [23,24], nanorings [25], rods [26], hollow spheres [27] and nanorhombohedra [28] have been fabricated, and their various functions have been tested. Controlling the morphology in the synthesis of α-Fe_2O_3 hierarchical structures has thus become the major synthetic goal. Lately, Cao et al. [29] described a facile route for the preparation of α-Fe_2O_3 micro-pine microcrystals. Hu et al. [30] obtained α-Fe_2O_3 snowflake hierarchical structures on a large scale in an efficient microwave-assisted hydrothermal process. Gong's group [31] has synthesized α-Fe_2O_3 crystals with different morphologies by changing the pH value in an aqueous reaction system. In all these processes, $[Fe(CN)_6]^{3-}$ ions were used as a single iron source for the slow generation of Fe^{3+} ions under a hydrothermal condition. However, it is still not easy to control the morphology and photocatalytic properties of the α-Fe_2O_3 crystals systematically using only one iron precursor. Developing a simple and more accurate method to synthesize α-Fe_2O_3 crystals with various morphologies is still in need.

Herein, a dual iron precursors system was developed for the controllable synthesis of α-Fe_2O_3 hierarchical structures. Metal complexes, $[Fe(CN)_6]^{4-}$ and $[Fe(CN)_6]^{3-}$ in this work, usually can provide a proper environment for the generation of novel structures based on their flexible coordination modes in the synthetic progress [29–31]. α-Fe_2O_3 hierarchical structures with different morphologies (micro-pine, snowflake and bundles) were successfully fabricated simply by tuning the total concentration of the two iron precursors and their molar ratio in a hydrothermal process. A possible formation mechanism of different α-Fe_2O_3 hierarchical structures was also proposed. Meanwhile, the photocatalytic

* Corresponding author. Fax: +86 431 85098787.
E-mail addresses: wangeb889@nenu.edu.cn, wangenbo@public.cc.jl.cn (E. Wang).

0022-4596/$ - see front matter © 2009 Published by Elsevier Inc.
doi:10.1016/j.jssc.2009.01.041

property of the α-Fe_2O_3 hierarchical structures was investigated in the photocatalytic degradation of salicylic acid.

2. Experimental section

2.1. Materials

All chemicals, $K_3[Fe(CN)_6]$, $K_4[Fe(CN)_6] \cdot 3H_2O$ and salicylic acid are of analytical grade and used as received without further purification.

2.2. Synthesis

A typical synthesis procedure of the α-Fe_2O_3 snowflake hierarchical structure was as follows: 0.6 mmol $K_4[Fe(CN)_6] \cdot 3H_2O$ and 0.12 mmol $K_3[Fe(CN)_6]$ (the molar ratio of $K_4[Fe(CN)_6]$/$K_3[Fe(CN)_6]$ was 5) were dissolved in 12 mL distilled water under magnetic stirring for 40 min at room temperature until a yellow transparent solution appeared. Then, the yellow solution was transferred into a 15 mL Teflon-lined autoclave and sealed. After hydrothermally treated at 140 °C for 48 h, the autoclave was cooled to room temperature naturally. Finally, the final products were separated by centrifugation, washed with distilled water and absolute ethanol repeatedly before oven drying at 60 °C for 24 h.

The synthesis procedures of α-Fe_2O_3 micro-pine and bundles hierarchical structures were similar as that of the snowflake hierarchical structure except that the total concentration of the two iron precursors and their molar ratio were changed. These reactions were easily repeated, and the resulted structures were highly stable. No morphology or composition change was observed over several months when stored in air or absolute ethanol.

2.3. Characterization

Transmission electron microscopy (TEM, Hitachi-7500, operating voltage of 120 kV) and field-emission scanning electron microscopy (FESEM, XL30, Philips, operating voltage of 20 kV) were used to observe the morphologies of the final products. X-ray diffraction patterns (XRD) were measured using a Rigaku D/max-IIB X-ray diffractometer at a scanning rate of 4°/min with 2θ ranging from 10° to 90°, using Cu$K\alpha$ radiation ($\lambda = 1.5418$ Å). The chemical compositions were studied using X-ray photoelectron spectroscopy (XPS) and energy-dispersive X-ray analysis (EDX). A Hitachi F-4500 fluorophotometer was used in the study of the photocatalytic property of α-Fe_2O_3 structures.

2.4. Photocatalysis experiments

In a typical process, 20 mg of α-Fe_2O_3 hierarchical structures and 5 mg of salicylic acid were dissolved in 50 mL distilled water and then magnetically stirred in the dark for 50 min to generate a good dispersion and to establish the adsorption–desorption equilibrium between the organic molecules and the catalyst surface. The solution was then exposed to UV irradiation from a 125 W Hg lamp at a distance of 3–4 cm between the liquid surface and the lamp. The solution was stirred with a magnetic stir bar during irradiation. In total, 2 mL of samples were taken out from the beaker at different time intervals. After α-Fe_2O_3 was removed using centrifugation and filtration, the solution was used for fluorescence analysis. The emission intensity of salicylic acid at 412 nm was monitored with the excitation wavelength at 296 nm.

3. Results and discussion

3.1. Characterizations of α-Fe_2O_3 micro-pine hierarchical structure

Fig. 1 shows the FESEM images with different magnifications of the α-Fe_2O_3 micro-pine hierarchical structures synthesized when the concentration of $K_4[Fe(CN)_6]$ was 0.01 M and the molar ratio of $K_4[Fe(CN)_6]$/$K_3[Fe(CN)_6]$ was 1/5. The low-magnification image in Fig. 1a shows that the products have regular micro-pine structures. Fig. 1b reveals the difference between the two surfaces of one micro-pine structure. Micro-pine hierarchical structures

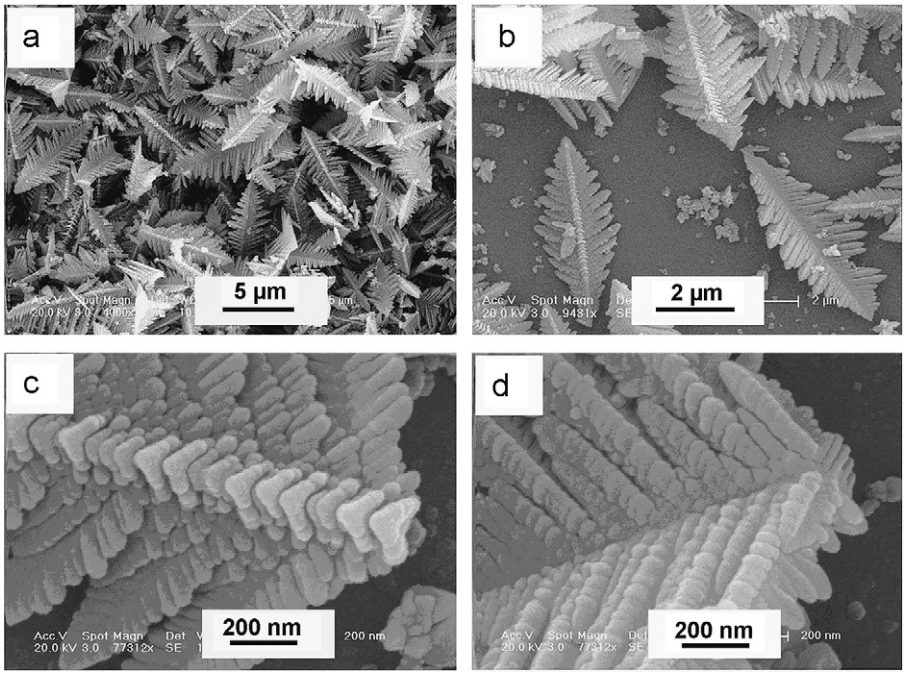

Fig. 1. FESEM images of micro-pine hierarchical structures prepared when the concentration of $K_4[Fe(CN)_6]$ was 0.01 M and the molar ratio of $K_4[Fe(CN)_6]$/$K_3[Fe(CN)_6]$ was 1/5: (a) panorama of micro-pine; (b) micro-pine in two opposite directions; high-magnification FESEM image of a single micro-pine in one direction (c) and (d) in the opposite direction.

with a clear central trunk and highly ordered parallel branches distributed on both sides of the trunk are obviously observed. The length of the central trunks is about 4.5 μm, and that of the branch trunk ranges from 100 nm to 1.5 μm. The high-magnification images in Fig. 1c and d show the details of the trunk and branches. The central trunk is composed of orderly arranged trigonal particles with sizes being about 200 nm (Fig. 1c). All the branch trunks consist of regular nanoparticles with sizes of about 100 nm (Fig. 1d). Parallel nanorods (100–200 nm) can be defined as the subunits of the branches.

A typical TEM image of α-Fe_2O_3 micro-pines is shown in Fig. 2a. The length of the central trunks is about 4.5 μm, in agreement with the observation from FESEM images (Fig. 1b). Fig. 2b and the inset show the morphology of a broken α-Fe_2O_3 micro-pine hierarchical structure. The SAED pattern of the products demonstrates that the α-Fe_2O_3 micro-pine structures are single crystalline (Fig. 2c).

The composition and phase purity of the samples were examined using XRD. Fig. 3 shows the typical XRD pattern of the micro-pine hierarchical structure. According to the reflection peak positions and relative intensities, the pattern is in good agreement with the literature values and can be indexed to the hexagonal phase of α-Fe_2O_3 (hematite) ($a = 5.035$ Å, $c = 13.740$ Å, JCPDS no. 33-0664) with no other peaks of impurities detected.

3.2. Characterizations of α-Fe_2O_3 snowflake hierarchical structure

Sixfold-symmetric α-Fe_2O_3 snowflake hierarchical structures were obtained when the concentration of $K_4[Fe(CN)_6]$ was 0.05 M and the molar ratio of $K_4[Fe(CN)_6]/K_3[Fe(CN)_6]$ was 5/1, as seen from the low-magnification FESEM image (Fig. 4a). The individual α-Fe_2O_3 snowflake hierarchical structure as shown in Fig. 4b consists of self-assembled sixfold-symmetric dendritic branch with the average length of each trunk being about 4.5 μm. The intersect angle of the adjacent branches is 60°. Fig. 4c shows orderly arranged nanorods with the length of about 200–700 nm grow on the both sides of a trunk and are parallel to each other. Energy-dispersive X-ray analysis shown in Fig. 4d proves the presence of Fe and O in the α-Fe_2O_3 snowflake hierarchical structure. The peaks corresponding to the Si atom and Au atom, respectively, come from the silicon substrate and sprayed gold.

The morphology of the α-Fe_2O_3 snowflakes was also investigated by TEM (Fig. 5). Fig. 5a shows a typical TEM image of an individual symmetric α-Fe_2O_3 snowflake hierarchical structure, giving a further insight into the morphology (Fig. 4b). The TEM image of an asymmetric α-Fe_2O_3 snowflake hierarchical structure is also given in Fig. 5b. The SAED pattern (Fig. 5c) suggests that the α-Fe_2O_3 snowflake hierarchical structure is single crystalline.

Fig. 6 shows the typical XRD pattern of the snowflake hierarchical structures. According to the reflection peak positions and relative intensities, the pattern is in good agreement with the literature values and can be easily indexed to the hexagonal phase of α-Fe_2O_3 (hematite) ($a = 5.035$ Å, $c = 13.740$ Å, JCPDS no. 33-0664) with no other peaks of impurities detected. Furthermore, the surface electronic states and the chemical composition of the product are examined using XPS. In the high-resolution Fe 2*p* spectrum (Fig. 7), two peaks at binding energies of about 711 eV for Fe $2p_{3/2}$ and about 724 eV for Fe $2p_{1/2}$ with a shakeup satellite at about 719 eV prove the presence of Fe (β) in α-Fe_2O_3 [32].

3.3. Characterizations of α-Fe_2O_3 bundles hierarchical structure

Fig. 8 shows the FESEM images of α-Fe_2O_3 bundles hierarchical structures obtained when the concentration of $K_4[Fe(CN)_6]$ is 0.1 M and the molar ratio of $K_4[Fe(CN)_6]/K_3[Fe(CN)_6]$ is 1/8. The low-magnification FESEM image of the α-Fe_2O_3 bundles is shown in Fig. 8a. The high-magnification FESEM image (Fig. 8b) shows an individual α-Fe_2O_3 bundles structure, which is composed of parallel nanorods with diameters of about 160 nm and average lengths of several micrometers. TEM images are shown in Fig. 9a. The SAED pattern (Fig. 9b) indicates the single-crystalline nature of the samples.

Fig. 10 shows the typical XRD pattern of the samples. According to the reflection peak positions and relative intensities, the pattern is in good agreement with the literature values and can be easily indexed to the hexagonal phase of α-Fe_2O_3 (hematite) ($a = 5.035$ Å, $c = 13.740$ Å, JCPDS no. 33-0664) with no other peaks of impurities detected.

3.4. The effect of experimental conditions on the morphologies of the α-Fe_2O_3 crystals

To study the effect of experimental conditions on the morphologies of the α-Fe_2O_3 crystals, series of control experiments were

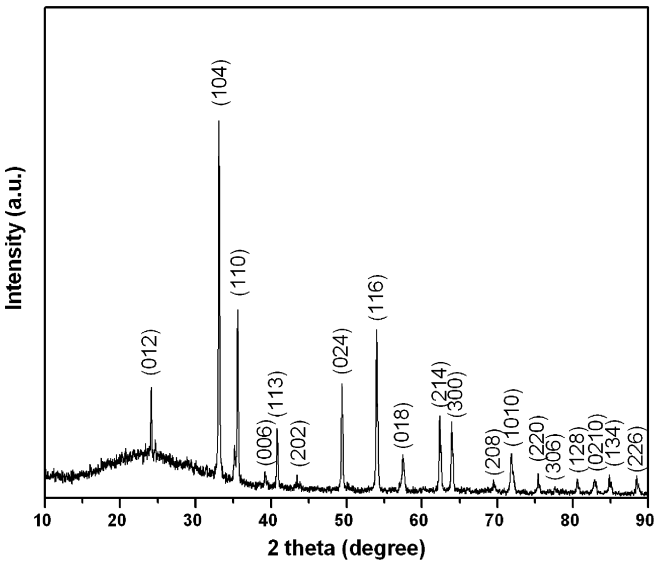

Fig. 3. XRD pattern of the sample prepared when the concentration of $K_4[Fe(CN)_6]$ was 0.01 M and the molar ratio of $K_4[Fe(CN)_6]/K_3[Fe(CN)_6]$ was 1/5 at 140 °C for 48 h.

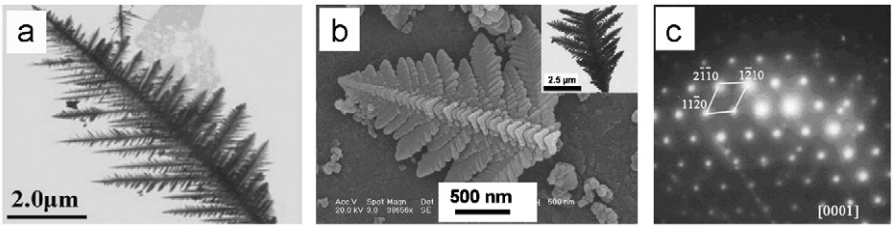

Fig. 2. (a) TEM image of a single micro-pine; (b) SEM image and TEM (inset) of a broken micro-pine and (c) SAED pattern of micro-pine.

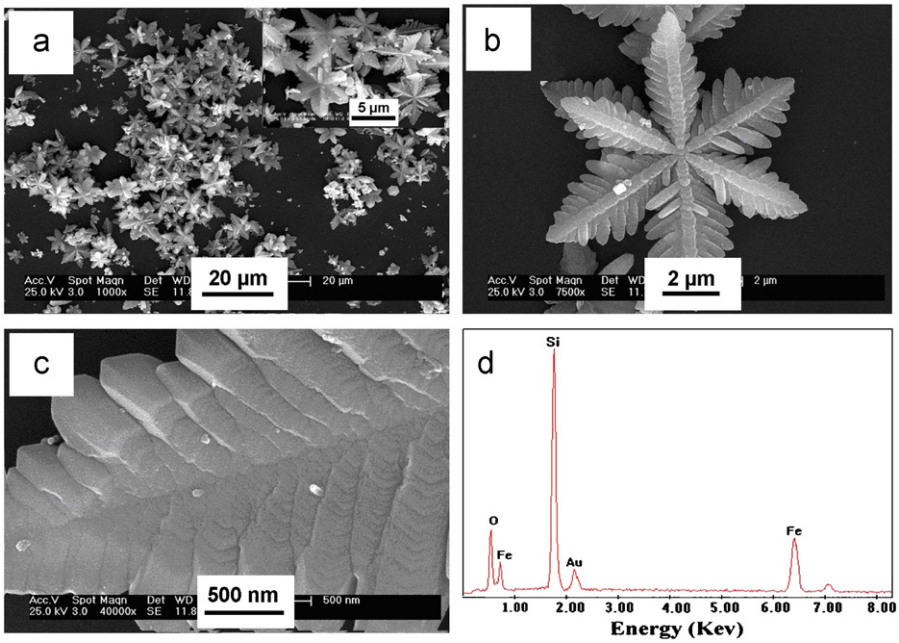

Fig. 4. FESEM images of snowflake hierarchical structures prepared when the concentration of $K_4[Fe(CN)_6]$ was 0.05 M and the molar ratio of $K_4[Fe(CN)_6]/K_3[Fe(CN)_6]$ was 5/1: (a) panorama of snowflake; (b) single snowflake; (c) high-magnification FESEM image of the one petal of a snowflake and (d) EDS pattern of snowflake.

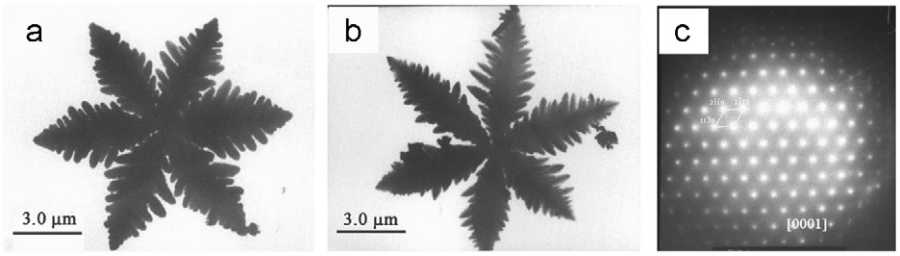

Fig. 5. (a) TEM image of a single snowflake; (b) asymmetric shape of a snowflake and (c) SAED pattern of snowflake.

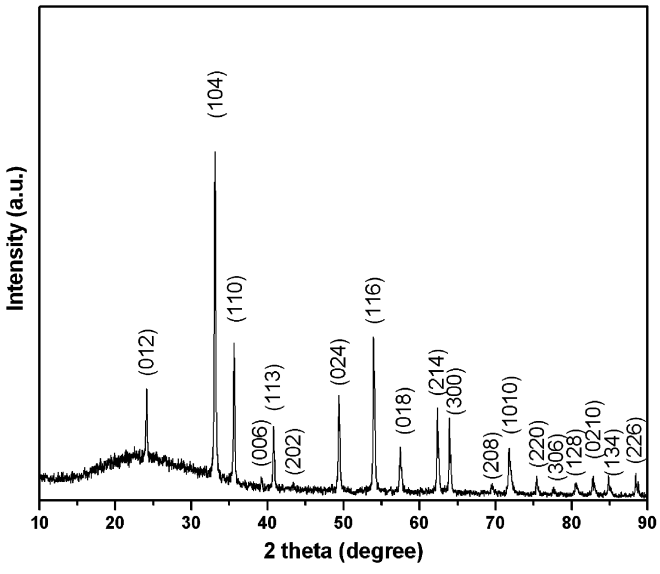

Fig. 6. XRD pattern of the sample prepared when the concentration of $K_4[Fe(CN)_6]$ was 0.05 M and the molar ratio of $K_4[Fe(CN)_6]/K_3[Fe(CN)_6]$ was 5/1 at 140 °C for 48 h.

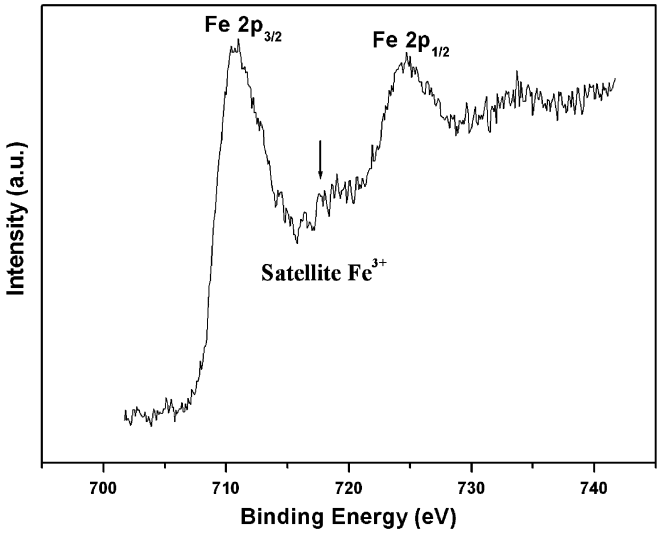

Fig. 7. XPS spectrum of Fe 2*p* of α-Fe_2O_3 snowflake.

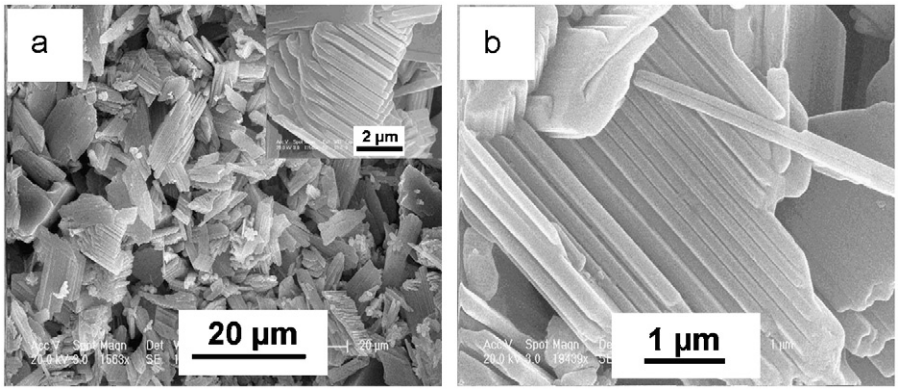

Fig. 8. FESEM images of bundles hierarchical structures prepared when the concentration of $K_4[Fe(CN)_6]$ was 0.1 M and the molar ratio of $K_4[Fe(CN)_6]/K_3[Fe(CN)_6]$ was 1/8: (a) panorama of bundles and (b) single bundles.

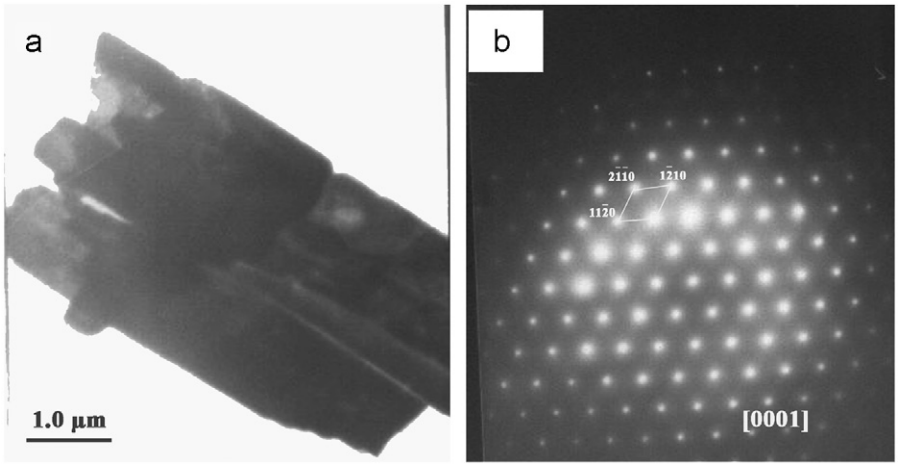

Fig. 9. (a) TEM image of single bundles and (b) SAED pattern of bundles.

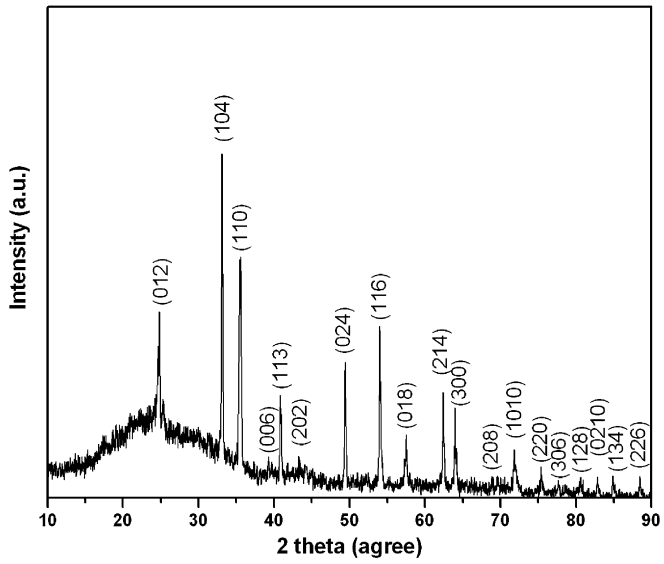

Fig. 10. XRD pattern of the sample prepared when the concentration of $K_4[Fe(CN)_6]$ was 0.1 M and the molar ratio of $K_4[Fe(CN)_6]/K_3[Fe(CN)_6]$ was 1/8 at 140 °C for 48 h.

carried out with the total concentration of the two iron precursors ranging from 0.01 to 1.0 M and their molar ratio increased in a systematic way. When the total concentration of the two iron precursors was kept at 0.08 M and their molar ratio was changed, micro-pine hierarchical structures precipitated out when the molar ratio of $K_4[Fe(CN)_6]/K_3[Fe(CN)_6]$ was 1/7 (Fig. 11a) or 2/6; micro-pine hierarchical structures with some α-Fe_2O_3 snowflake hierarchical structures came out at the same time when the molar ratio of $K_4[Fe(CN)_6]/K_3[Fe(CN)_6]$ was 3/5, 4/4 or 5/3; when the molar ratio of $K_4[Fe(CN)_6]/K_3[Fe(CN)_6]$ was 6/2 (Fig. 11b) or 7/1, snowflake hierarchical structures were predominant in the products. When the total concentration of the two iron precursors was kept at 0.8 M and the molar ratio was varied, bundles instead of micro-pines or snowflakes were obtained when the molar ratio of $K_4[Fe(CN)_6]/K_3[Fe(CN)_6]$ was 1/7 (Fig. 11c), 2/6, 3/5 and 4/4; when the molar ratio of $K_4[Fe(CN)_6]/K_3[Fe(CN)_6]$ was changed to 5/3 (Fig. 11d), 6/2 or 7/1, the product appeared to be unformed snowflakes.

Based on these observations, when the total concentration of the two iron precursors and their molar ratio were changed, the morphology of α-Fe_2O_3 crystal can be tuned to micro-pine, snowflake, bundles and unformed snowflakes. Thus, we believe that the total concentration of the two iron precursors and their molar ratio play a crucial role on controlling the morphology of α-Fe_2O_3 crystal.

3.5. Formation mechanisms of different α-Fe_2O_3 hierarchical structures

3.5.1. α-Fe_2O_3 micro-pine and snowflake hierarchical structures

$[Fe(CN)_6]^{3-}$ and $[Fe(CN)_6]^{4-}$, with the standard equilibrium constant are 1.0×10^{42} and 1.0×10^{35}, respectively, are both stable

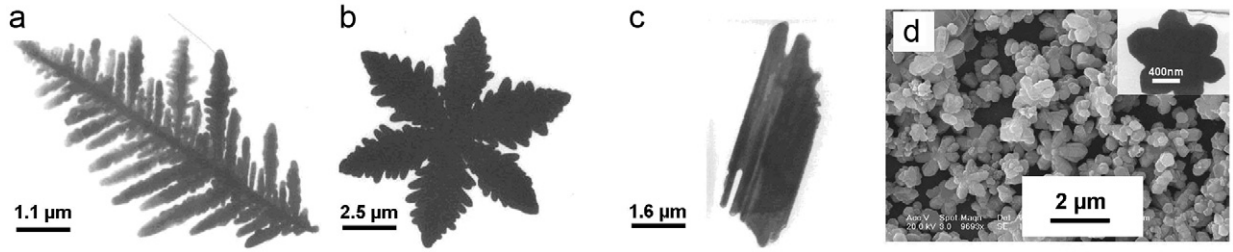

Fig. 11. (a) Single micro-pine prepared when the concentration of $K_4[Fe(CN)_6]$ was 0.01 M and the molar ratio of $K_4[Fe(CN)_6]/K_3[Fe(CN)_6]$ was 1/7; (b) single snowflake prepared when the concentration of $K_4[Fe(CN)_6]$ was 0.06 M and the molar ratio of $K_4[Fe(CN)_6]/K_3[Fe(CN)_6]$ was 6/2; (c) single bundles prepared when the concentration of $K_4[Fe(CN)_6]$ was 0.1 M and the molar ratio of $K_4[Fe(CN)_6]/K_3[Fe(CN)_6]$ was 1/7; and (d) panorama of unformed snowflake prepared when the concentration of $K_4[Fe(CN)_6]$ was 0.5 M and the molar ratio of $K_4[Fe(CN)_6]/K_3[Fe(CN)_6]$ was 5/3.

in the aqueous solution and almost no free Fe^{3+} ions can be detected at room temperature. Obviously, $[Fe(CN)_6]^{4-}$ exhibits lower stability than $[Fe(CN)_6]^{3-}$ in the aqueous solution. Considering different stability, if the two iron precursors ($K_3[Fe(CN)_6]$ and $K_4[Fe(CN)_6]$) are employed to the same reaction system, whether any novel α-Fe_2O_3 structure could be obtained.

A three-step formation mechanism of the different structures was proposed in Scheme 1. First, the Fe^{3+} ions were generated from slowly dissociation from $[Fe(CN)_6]^{3-}$ as well as from the oxidation of Fe^{2+} ions dissociated slowly from $[Fe(CN)_6]^{4-}$ by the dissolved oxygen. Then all the Fe^{3+} ions were hydrolyzed in aqueous solutions and FeOOH or $Fe(OH)_3$ were generated. FeOOH or $Fe(OH)_3$ was finally decomposed to form α-Fe_2O_3 crystals.

Based on the results from the control experiments, the employment of a small amount of $K_4[Fe(CN)_6]$ cannot be enough to affect the generation rate of the Fe^{3+} ions in the entire system. Only α-Fe_2O_3 micro-pine hierarchical structures could be obtained when both the concentration of $K_4[Fe(CN)_6]$ and their molar ratio were low (Fig. 11a). A mature formation mechanism of α-Fe_2O_3 micro-pine hierarchical structures obtained via a single iron precursor $K_3[Fe(CN)_6]$ has been proposed in a previous research [29]. Herein, a possible formation process of α-Fe_2O_3 micro-pine hierarchical structures is demonstrated in Fig. 12. The crystal structure (Fig. 12e) shows that $\langle 10\bar{1}0 \rangle$ are six equivalent directions. However, due to spatial confinement, one of the directions, such as $[1\bar{1}00]$, could initiate fast growth. It is possible to form a needle if the growth along $[1\bar{1}00]$ is much faster than along the other directions (Fig. 12a). Subsequent growth along the other two crystallographically equivalent directions ($[10\bar{1}0]$ and $[01\bar{1}0]$) may result in the formation of symmetric branches on both sides (Fig. 12b). With further growth, each side branch can also grow along $\pm[01\bar{1}0]$ and $\pm[10\bar{1}0]$ to minibranches (Fig. 12c) and finally α-Fe_2O_3 micro-pine hierarchical structures are obtained (Fig. 2a).

When the amounts of $K_4[Fe(CN)_6]$ in the reaction systems were relatively increased, the morphology of α-Fe_2O_3 nano-crystals changed from micro-pine (Fig. 11a) to snowflake (Fig. 11b). A possible reason for the morphology change was that the generation rate of Fe^{3+} ions as well as the generation rate of $FeOOH/Fe(OH)_3$ would increase dramatically. Thus, the tendency of growth along the six crystallographically equivalent directions $\langle 10\bar{1}0 \rangle$ would increase due to the increase of the kinetic factor and the breaking of the limit on the spatial confinement of the crystal growth. The growth of α-Fe_2O_3 snowflake hierarchical structures along $[10\bar{1}0]$ and $[01\bar{1}0]$ directions could also increase [31]. As growth continues, all of the branches became thicker and finally interconnected to form a compact snowflake (Fig. 12d). Based on the above-mentioned ratiocination, the increase of

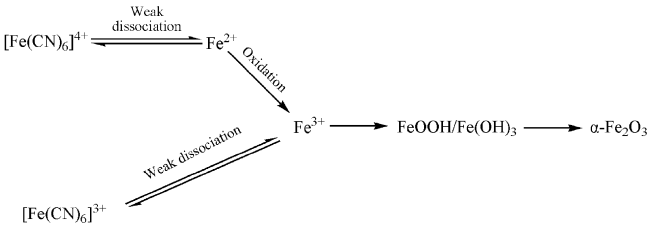

Scheme 1. Schematic process for synthesis of the α-Fe_2O_3 hierarchical structures.

$K_4[Fe(CN)_6]$ played a crucial role in the formation process of α-Fe_2O_3 snowflake hierarchical structures.

Generally, as previous literature reported [33], hierarchical structures are formed through a self-assembly process under non-equilibrium conditions. Small bumps on the surface of a growing crystal develop into large branches, and bumps on the branches become side branches. Once branching instability applies itself to a growing crystal, the dendrite structures are formed. This instability plays a vital role in obtaining the complex structures of the α-Fe_2O_3 crystals. In solution growth system, once the initial α-Fe_2O_3 crystals are formed, further coarsening needs further diffusion of the α-Fe_2O_3 crystals, which can slow the crystal growth rate and then the morphology could be controlled. When the diffusion of the bumps reaches the initial nucleated crystals faster, bulk growth tends to be easier. For instance, in our experiments obtaining snowflakes, large amounts of $[Fe(CN)_6]^{4-}$ are employed, the generation rate of Fe^{3+} ions increases and the diffusion rate of subsequent formed α-Fe_2O_3 will also increase. The probability to attach simultaneously onto the six equivalent facets of the initial crystals leads to the α-Fe_2O_3 snowflake hierarchical structures.

3.5.2. α-Fe_2O_3 bundles hierarchical structures

In principle, the growth process of crystals consists of an initial nucleating step and a subsequent growth step. α-Fe_2O_3 is a polar crystal, and the Fe^{3+} and O^{2-} ions are arranged alternatively parallel to the (0001) plane [29]. The concentration is also a critical factor for the crystalline phase of the nuclei and the growth rate of the different crystal surfaces [34]. Thus, when the total concentration of the two iron precursors is rather high, the nucleation would be so rapid that more α-Fe_2O_3 nuclei form in the chemical systems. With the preferential growth along the (0001) direction proceeding, α-Fe_2O_3 nanorods would appear in the products. Subsequently, these nanorods aggregate and grow into bundles due to excess saturation. The formation of α-Fe_2O_3 bundles involves spontaneous assembly and coalescence of

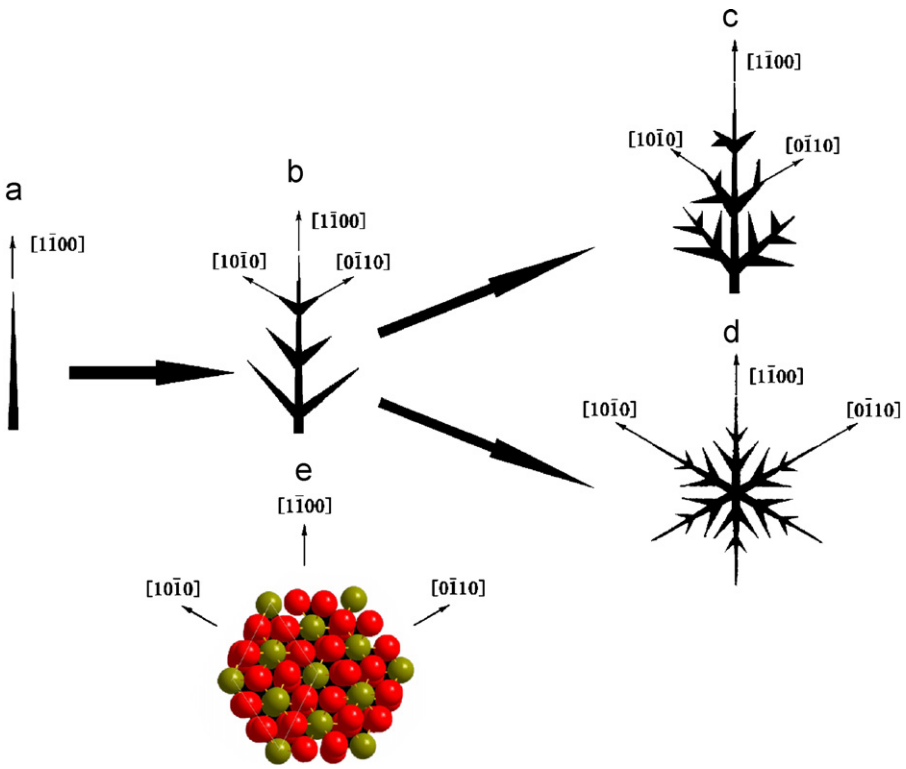

Fig. 12. Proposed growth processes of α-Fe_2O_3 micro-pine and snowflake.

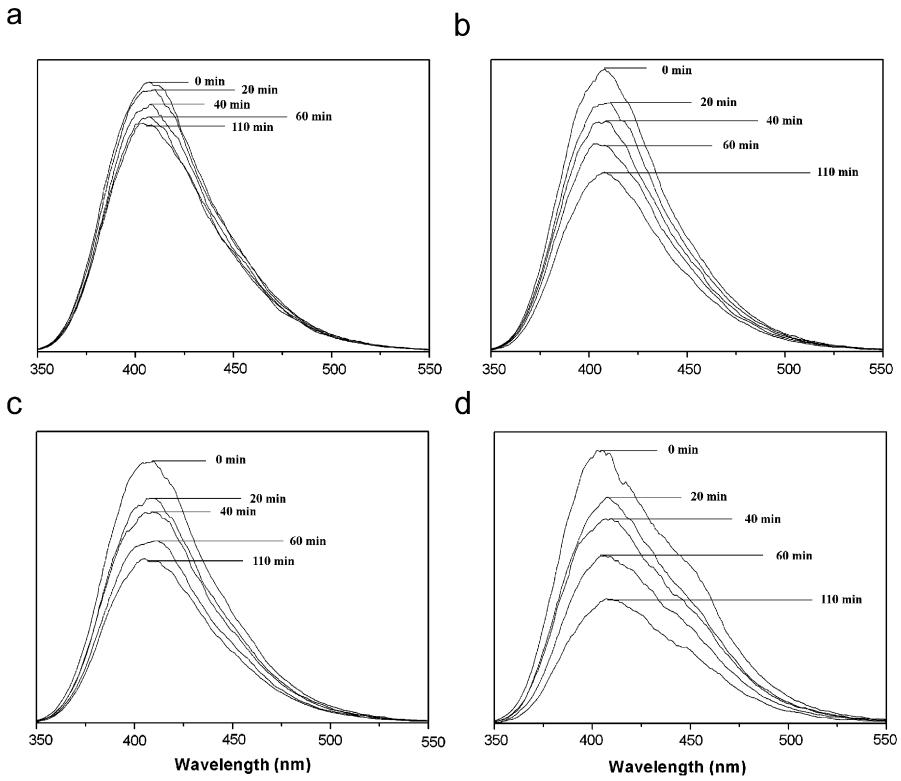

Fig. 13. Change in fluorescence intensity of salicylic acid (100 mg L^{-1}): (a) direct photocatalysis; (b) in the presence of 20 mg α-Fe_2O_3 snowflake; (c) in the presence of 20 mg α-Fe_2O_3 micro-pine and (d) in the presence of 20 mg α-Fe_2O_3 bundles.

adjacent nanorods so that the surface energy could be reduced. We must acknowledge that the exact mechanism for the formation of α-Fe_2O_3 bundles hierarchical structures is still unclear. However, it is obvious that higher concentrations of the two iron precursors are of great importance in the growth of α-Fe_2O_3 bundles hierarchical structures.

3.6. Photocatalytic properties of different α-Fe_2O_3 hierarchical structures

The photocatalytic performance of the α-Fe_2O_3 hierarchical structures with different morphologies (micro-pine, snowflake and bundles) was investigated with photocatalytic degradation of salicylic acid. The reference of salicylic acid without any photocatalyst was tested for comparison. The monitored fluorescence spectra of salicylic acid were shown in Fig. 13 when different α-Fe_2O_3 hierarchical structures were used as photocatalysts. The fluorescence intensities of the salicylic acid solution decreased obviously upon irradiation, confirming the photocatalytic property of the α-Fe_2O_3 hierarchical structures. Moreover, the conversions in the concentration of salicylic acid (K) versus reaction time (t) were plotted in Fig. S1 (in the Supplemental data). The conversion of salicylic acid (K) can be expressed as $K = (I_0 - I_t)/I_0$, where I_0 represents the fluorescence intensity of salicylic acid at the original reaction ($t = 0$), while I_t is the fluorescence intensity at a specific irradiation time t. It can be further confirmed that the samples showed good photocatalytic properties in the photocatalytic degradation of salicylic acid.

4. Conclusions

In summary, a hydrothermal process with a dual iron precursors system was developed for controllable fabrication of α-Fe_2O_3 hierarchical structures (micro-pine, snowflake and bundles) on a large scale. It is found that the total concentration of the two iron precursors ($K_4[Fe(CN)_6]$ and $K_3[Fe(CN)_6]$) and their molar ratio played a crucial role in the morphology control of the hierarchical structures. A possible formation mechanism of different α-Fe_2O_3 hierarchical structures was proposed. The photocatalytic degradation of salicylic acid study verified the photocatalytic properties of the α-Fe_2O_3 hierarchical structures. This easily manipulated method may be useful for the large-scale synthesis of other materials, especially transition-metal oxides.

Supplementary data

Supplementary data provides the figure about plot of the conversions in the concentration of salicylic acid versus reaction time.

Acknowledgments

This work was supported by the National Natural Science Foundation of China (nos. 20701005/20701006), the Science and Technology Development Project Foundation of Jilin Province (no. 20060420), the Postdoctoral station Foundation of Ministry of Education (no. 20060200002), the Testing Foundation of Northeast Normal University and the Program for Changjiang Scholars and Innovative Research Team in University.

Appendix A. Supplementary material

Supplementary data associated with this article can be found in the online version at doi:10.1016/j.jssc.2009.01.041.

References

[1] J.S. Hu, L.S. Zhong, W.G. Song, L.J. Wan, Adv. Mater. 20 (2008) 2977–2982.
[2] A. Sukhanova, A.V. Baranov, T.S. Perova, J.H.M. Cohen, I. Nabiev, Angew. Chem. Int. Ed. 45 (2006) 2048–2052.
[3] L.H. Lu, A. Kobayashi, Y. Kikkawa, K. Tawa, Y. Ozaki, J. Phys. Chem. B 110 (2006) 23234–23241.
[4] T.R. Zhang, W.J. Dong, M. Keeter-Brewer, S. Konar, R.N. Njabon, Z.R. Tian, J. Am. Chem. Soc. 128 (2006) 10960–10968.
[5] D. Moore, Y. Ding, Z.L. Wang, Angew. Chem. Int. Ed. 45 (2006) 5150–5154.
[6] R.H. Jin, J.J. Yuan, Chem. Commun. (2005) 1399–1401.
[7] L. Ye, C.Z. Wu, W. Guo, Y. Xie, Chem. Commun. (2006) 4738–4740.
[8] S.N. Mlondo, E.M. Andrews, P.J. Thomas, P. O'Brien, Chem. Commun. (2008) 2768–2770.
[9] J.Y. Lao, J.Y. Huang, D.Z. Wang, Z.F. Ren, Nano Lett. 3 (2003) 235–238.
[10] G.R. Li, C.Z. Yao, X.H. Lu, F.L. Zheng, Z.P. Feng, X.L. Yu, C.Y. Su, Y.X. Tong, Chem. Mater. 20 (2008) 3306–3314.
[11] Z.W. Pan, Z.R. Dai, Z.L. Wang, Science 291 (2001) 1947–1949.
[12] Y.S. Ding, X.F. Shen, S. Gomez, H. Luo, M. Aindow, S.L. Suib, Adv. Funct. Mater. 16 (2006) 549–555.
[13] M. Siskin, A.R. Katritzky, Science 254 (1991) 231–237.
[14] X. Wang, J. Zhuang, Q. Peng, Y.D. Li, Nature 437 (2005) 121–124.
[15] M. Anderman, J.H. Kennedy, in: H.O. Finklea (Ed.), Semiconductor Electrodes, Elsevier, Amsterdam, 1988.
[16] L.L. Li, Y. Chu, Y. Liu, L.H. Dong, J. Phys. Chem. C 111 (2007) 2123–2127.
[17] C.Z. Wu, P. Yin, X. Zhu, C.Z. Ou Yang, Y. Xie, J. Phys. Chem. B 110 (2006) 17806–17812.
[18] S.Y. Zeng, K.B. Tang, T.W. Li, Z.H. Liang, D. Wang, Y.K. Wang, Y.X. Qi, W.W. Zhou, J. Phys. Chem. C 112 (2008) 4836–4843.
[19] Y.Y. Xu, X.F. Rui, Y.Y. Fu, H. Zhang, Chem. Phys. Lett. 410 (2005) 36–38.
[20] L.P. Zhu, H.M. Xiao, X.M. Liu, S.Y. Fu, J. Mater. Chem. 16 (2006) 1794–1797.
[21] Y.H. Zheng, Y. Cheng, Y.S. Wang, F. Bao, L.H. Zhou, X.F. Wei, Y.Y. Zhang, Q. Zheng, J. Phys. Chem. B 110 (2006) 3093–3097.
[22] X.G. Wen, S.H. Wang, Y. Ding, Z.L. Wang, S.H. Yang, J. Phys. Chem. B 109 (2005) 215–220.
[23] L. Liu, H.Z. Kou, W.L. Mo, H.J. Liu, Y.Q. Wang, J. Phys. Chem. B 110 (2006) 15218–15223.
[24] C.J. Jia, L.D. Sun, Z.G. Yan, L.P. You, F. Luo, X.D. Han, Y.C. Pang, Z. Zhang, C.H. Yan, Angew. Chem. Int. Ed. 44 (2005) 4328–4333.
[25] C.J. Jia, L.D. Sun, F. Luo, X.D. Han, L.J. Heyderman, Z.G. Yan, C.H. Yan, K. Zheng, Z. Zhang, M. Takano, N. Hayashi, M. Eltschka, M. Klaui, U. Rudiger, T. Kasama, L. Cervera-Gontard, R.E. Dunin-Borkowski, G. Tzvetkov, J. Raabe, J. Am. Chem. Soc. 130 (2008) 16968–16977.
[26] B. Tang, G.L. Wang, L.H. Zhuo, J.C. Ge, L. Cui, J. Inorg. Chem. 45 (2006) 5196–5200.
[27] B.D. Mao, Z.H. Kang, E.B. Wang, C.G. Tian, Z.M. Zhang, C.L. Wang, Y.L. Song, M.Y. Li, J. Solid State Chem. 180 (2007) 497–503.
[28] Z.F. Pu, M.H. Cao, J. Yang, K.L. Huang, C.W. Hu, Nanotechnology 17 (2006) 799–804.
[29] M.H. Cao, T.F. Liu, S. Gao, G.B. Sun, X.L. Wu, C.W. Hu, Z.L. Wang, Angew. Chem. Int. Ed. 44 (2005) 4197–4201.
[30] X.L. Hu, J.C. Yu, J.M. Gong, J. Phys. Chem. C 111 (2007) 11180–11185.
[31] X.L. Zhang, C.H. Sui, J. Gong, Z.M. Su, L.Y. Qu, J. Phys. Chem. C 111 (2007) 9049–9054.
[32] N.S. Mcintyre, D.G. Zetaruk, Anal. Chem. 49 (1977) 1521–1529.
[33] H. Imai, Top. Curr. Chem. 270 (2007) 43–72.
[34] Q. Peng, Y.J. Dong, Z.X. Deng, Y.D. Li, Inorg. Chem. 41 (2002) 5249–5254.